Article Type (Full Paper)

Wettability Behavior of Solution Blow Spun Polysulfone by Controlling Morphology

José E. Domínguez, Ali Kasiri, Javier González-Benito*

_____

José E. Domínguez
Universidad Tecnológica del Centro de Veracruz, Cuitláhuac, Veracruz, México.
E-mail: jose.dominguez@utcv.edu.mx

Ali Kasiri
Dept. Materials Science and Engineering and Chemical Engineering, Universidad Carlos III de Madrid, 28911-Leganés, Madrid, Spain.
E-mail: akasiri@pa.uc3m.es

Dr. Javier González-Benito*
Dept. Materials Science and Engineering and Chemical Engineering, IQMAAB, Universidad Carlos III de Madrid, 28911-Leganés, Madrid, Spain.
E-mail: javid@ing.uc3m.es

_____

Abstract:

Solution blow spinning, SBS, is used to prepare polysulfone materials, PSf, with different morphologies changing the processing conditions. Morphological study is done by scanning electron microscopy, SEM. Materials mainly constituted by beads and fibers are obtained. An optimization strategy based on desirability function approach together with Box-Behnken design is employed to find the best processing conditions to produce PSf materials with tailored morphology. Feed rate and air pressure are the variables of SBS processing conditions with the highest influence on the relative amount of fibers produced while air pressure and a particular balance between work distance and feed rate have the highest impact on the size of fibers. Contact angle measurements are used to understand SBS PSf wettability as a function of morphology.

It is demonstrated the possibility of designing PSf materials with particular wettability behavior induced by tailored morphologies obtained from a particular election of SBS processing conditions.

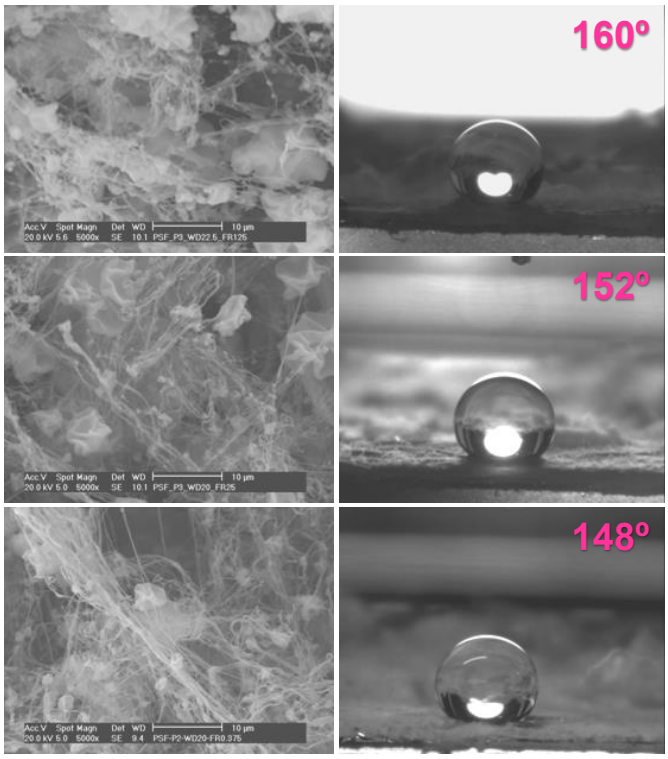

1. Introduction

Surface morphology of materials plays an important role in many applications. Most of them are related with wettability behavior in terms of adhesion and possible subsequent absorption processes. Among others, good wettability is required to improved coating processes while, poor wettability, leading to superhydrophobic surfaces, may help against biofilms formation for instance.

Although specific interactions condition wettability, other contributions like morphology might even have higher influence. In fact, well known hydrophilic materials with very heterogeneous surfaces may lead to very high water contact angles for instance.[1] Therefore, understanding the real mechanism by which a surface is wetted should be the prerequisite before designing supersolvophobic materials.

In general, when heterogeneous surfaces are considered, most of the researchers explain their wettabaility results by the consideration of the Cassie-Baxter approximation.[2] This approximation states a direct relation between the contact angle of a drop on a smooth surface, θ, and the contact angle on a rough surface, θ_r, using the well known equation, $\text{Cos}\ \theta_r = \varphi_1 \cos\theta - \varphi_2$. Where φ_1 and φ_2 are the fractions of solid surface and air that are in contact with the water droplet, respectively. Although many works try to explain their results from the Casie-Baxter expression, several times they seem to be no clear or even contradictory.[3] Therefore, higher efforts should be made in order to properly interpret wettability behavior of morphologically complex surfaces. For example, M. Al-Qadhi et al found that a polysulfone material made of non-woven fibers increased its hydrophobicity by decreasing the average diameter of the fibers. Taking into account Cassie-Baxter expression it could said that small diameter of the fibers should lead to

less surface contact with the liquid droplet.[3] However, this simple explanation does not seem to be enough to clearly understand the real wettability mechanism because, among other things, the relation between the material surface available and the dimensions of the fibers were not given.

On the other hand, apart from understanding the wettability mechanisms, preparing materials with well controlled morphologies is a very important issue in relation to their final applications. Nevertheless, only difficult and expensive micro and nanofabrication techniques allow successfully obtaining tailored morphologies.[4,5] Besides, these techniques usually lead to low scale productions, making them little attractive when low cost production is required. As a consequence, exploring new methods capable of giving materials with controlled morphologies at high rates of production would be of great importance.

Among the different possibilities in terms of morphology and unique characteristics such as large surface area, porosity, and versatility, the production of polymer-based materials constituted by submicrometer fibers has been a very attractive research field in the last decade. For instance, the use of fibers at micro or even nanoscale has been addressed to energy, biomedical, filtration, and other applications in recent years.[6]

Although there are different ways to produce non-woven fibers of thermoplastic materials, for example, melt spinning,[7] air blowing,[8] force spinning[9], dry-spinning[10] and electrospinning,[11] the method called solution blow spinning (SBS)[12] offers several advantages, for example, simplicity, low cost and high rate of fiber production.[13,14] Probably Electrospinning, ES, is the most studied technique to obtain materials for

biomedical proposes like for example scaffolds because, in general, more controlled morphologies can be obtained. On the other hand, dry-spinning, DS, is very similar to SBS. However, neither ES nor DS allow handling the device as to get the material *in-situ* in order, for instance, to be directly applied over a tissue to be repaired. In the particular case of ES mainly because a high electric field has to be applied while, in the case of DS because, portable devices are difficult to design and costs and heat inputs are usually very high.

SBS method is based mainly on the use of a concentric nozzle in which the inner channel extrudes a polymer solution while along the outer one pressurized gas is passed to push the polymer solution at the nozzle exit forming fibers that finally are deposited in a collector or substrate located at a particular working distance.[15] One of the most important things to take into account with SBS process is that there are different processing conditions that may condition the morphology of the material.[16] These processing conditions are characterized by certain solution parameters such as, viscosity, concentration and surface tension, as well as by operating parameters such as air pressure, feed rate and working distance. Therefore, in order to smartly prepared materials with tuned morphologies to finally condition their final performance, the SBS conditions should be smartly chosen and perfectly controlled.

Among the thermoplastic polymers, polysulfone (PSf) is a material with high mechanical strength and elongation to failure and excellent stability under hot and wet conditions. This polymer is gaining attention on medical applications as tissue replacement,[17] bone regeneration,[18] hemodialysis and apheresis,[19] among others. In fact, the National Surveillance of Dialysis-Associated reported that over 70% of

hemodialysis membranes are based on PSf.[20] Therefore, in order to widen the field of applications it seems to be reasonable to look for new ways of preparation of PSf-based materials with controlled morphologies. In particular, it is reported that fibers of polysulfone have been produced by electrospinning,[21] gas/jet-electrospinning[22] and air jet spinning or SBS.[23] However, in the particular case of SBS, as far as the authors know, there are not evidences of processing optimization to get PSf-based materials with controlled morphologies and their final relation with wettability behavior.

When individual factors and their interactions affect a specific response of a system, multi-response surface methodologies are usually useful. They combine mathematical and statistical approaches to fit empirical results with multiple linear regression from polynomial models to understand how certain result is influenced by those factors.[24,25] In fact, morphologies of several polymer systems produced by the SBS technique have been already optimized using a response surface methodology, for example, polylactic acid,[26,27] Zein biopolymer,[28] for which it was possible to know the influence of some SBS conditions on the diameter of the polymer fibers obtained.

The major role of experimental design concerns the method of optimization mainly focused on finding the experimental conditions required to produce the material with the best performance for a particular application.[29] On the other hand, design of experiments (DOE) does not necessary mean to use only one response. In fact, multi response optimization is needed many times; however, in those cases it is not possible to optimize each response separately. The overall solution respect to the best processing conditions must be included in an optimal range of values for the parameters that account for those experimental conditions.

Determination of the so-called desirability function is necessary to optimize multiple responses systems. This function is used to achieve the range of values of the parameters governing the processing conditions and finally design optimal experiments with maximum or minimum response values.[30] In fact, desirability function has been successfully used to optimize parameters in the manufacture of fibers by electrospinning.[31,32]

In this work, multi-response surface methodology is used to study the effects of three SBS experimental conditions on two responses (relative amount and size of fibers in terms of the ratio, RoF, and diameter of fibers, DoF, respectively) respect to the preparation of polysulfone materials. Multi-response optimization based on desirability value is employed to achieve the range of values of the experimental parameters chosen to obtain three different topographies. Finally, by studying the relation between the PSf morphologies and contact angles formed between a liquid and the surfaces generated, the wettability behavior is described from understanding the mechanisms of adhesion phenomena. This information will be of main importance to validate the multi-response surface method to optimize processing conditions to obtained tailored PSf morphologies with particular wettability performances.

2. Materials and methods

2.1. Materials

Polysulfone (PSf), Chemical structure I, in the form of pellets (M_w ~ 35000 g·mol^{-1} and M_n ~ 16000 g·mol^{-1}) was purchased from Sigma-Aldrich (Prod. No. 428302, Spain). Chloroform and acetone, supplied by Sigma-Aldrich (purity higher than 99.50 %), were

used to prepare the polymer solutions to be blow spun. All the materials were used as received without further purification.

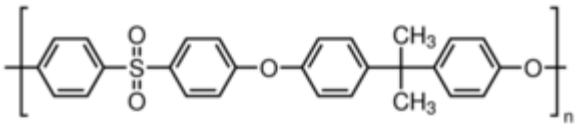

I, Chemical structure of polysulfone

2.2. Sample preparation

In order to prepare the polymeric solution, 1 g of PSF was carefully weighted out, added to 8 mL of chloroform, and stirred until full dissolution. After that, 2 mL of acetone was poured on the solution and the whole mixture was subjected to vigorous mechanical stirring for 20 minutes. Therefore, PSf polymer solution 10% (w/v) was prepared using a solvent formed by a mixture of chloroform/acetone (8:2, v/v).

The solution blow spinning, SBS, is a technique from which production of fibers is possible due to the interaction of two parallel fluid streams ejected from a concentric nozzle. In this particular work, a PSf solution was injected by a syringe using an automated pump (constituted by parts made of PLA with a 3D printer and works by the action of a piston driven by a stepper motor) to control the injection rate of the polymer solutions in the inner nozzle while pressurized air (pressure was controlled manually with pressure gauge and verified with other pressure gauge placed 10 cm from the nozzle). This sentence has been added to the experimental part in order to clarify.) is passed through the outer nozzle in order to transport the polymer solution at the output nozzle to finally reach a rotating drum (collector) located at a particular working distance (Figure 1). During flight, the polymer stretches while the solvent evaporates usually forming micro or even nanofibers.[12,15] The automated device used to prepare the materials was designed in our laboratory. All parts of the device were made in the

laboratory mainly with the use of a 3D printer. All the processing conditions, except the polymer solution characteristics, were directly set from and android device through the control established by an Arduino chip. The android device was a simple cell phone with the free app "BlueTerm" to control the Arduino chip through Bluetooth. The Arduino was programmed with the use of "Arduino IDE".

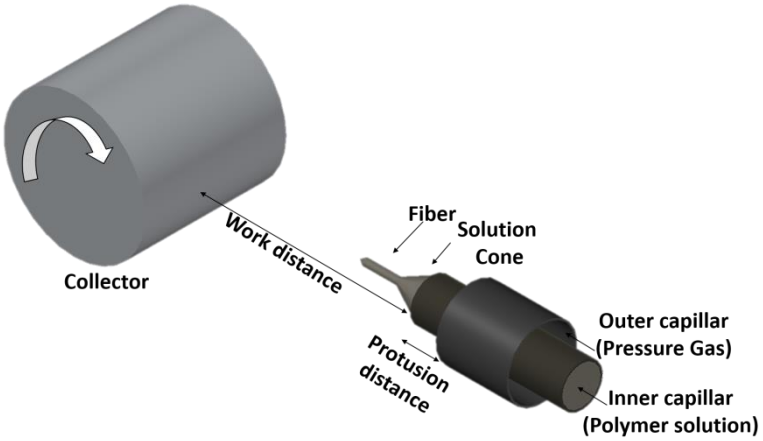

Figure 1. Concentric nozzle system and cylindrical collector used in SBS method.

The outer (OD) and inner (ID) diameters of the nozzle were 1 and 0.6 mm, respectively. The protrusion distance of inner nozzle was set at 2 mm respect to the concentric outer nozzle. PSf fibers were collected in a rotating cylinder of 63 mm of diameter at 200 rpm covered by an aluminum foil. In this study working distance, air pressure, and flow rate of the polymer solution were variable parameters associated to the SBS conditions to study their effect on a couple of morphological features, relative amount and diameter of fibers respectively. Working distances were chosen according to bibliography taking into account that most of the works using mixtures of chloroform-acetone point out that evaporation of solvent is ensured at 20 cm of working distance. On the other hand, after several previous experiments, range of air pressure was chosen above 1 bar in order to avoid nozzle blocking. Finally, feed rate range was chosen attending the most common values considered in the bibliography for similar polymer processing.

The temperature was kept constant at 24 ± 2 ºC during the production of all materials

2.3. Morphology study

The morphology of PSf samples was inspected by scanning electron microscopy, SEM, using a Phillips XL30 scanning electron microscope. As the acceleration voltage 20 kV were used and the SEM images were taken from the secondary electron signal. To avoid electrostatic charge accumulation the samples were gold coated by sputtering using a Leica EM ACE 200 Sputter coater using a current of 30 mA for 90 seconds.

The materials morphology features in terms of the relative amount of fibers, or ratio of fibers, RoF, and diameter of fibers, DF, were analyzed using the free image analysis software ImageJ V.1.52a, US (horizontal and vertical resolution of original image captured by SEM were 75 and 68 ppp respectively that corresponded in terms of pixels to 712 × 484 images). In particular, the RoF was calculated using the Equation (1) from the use of standardized images (700 × 400 pixels) where A_t is the total area of analysis A_{pe} the area covered by different micro-constituents like pearls or corpuscles and A_b the rest area of the image or the background (all areas are measured in pixels).

$$RoF = \frac{A_t - A_{pe} - A_{ba}}{A_t} \quad (1)$$

Every analyzed image was divided into four equal regions and then at least 20 independent and randomly chosen fibers were measured per region. Therefore, at least 80 measurements of diameters of fibers were made to carry out significant statistical treatments. Selection of fibers and other regions were carefully carried out by the operator. Only fibers clearly discernible with diameters higher than 50 nm were measured. All fibers measured were taken into account; only the black area corresponding to the label of the SEM image was discarded in the analysis.

Distribution of the diameter values were tested by traditional Anderson-Darling statistic (ADs) for normal fit while a modified ADs was used for lognormal, Weibull and Gamma fits to study how well data follow a specific distribution and then analyze the best statistical value representing the fiber diameter (average or median).

2.4. Data analysis

Box-Behnken response surface design (BBD) was used to determinate the effects of three factors on two independent morphological characteristics, the relative amount of fibers in terms of ratio of fibers respect to the rest of micro constituents (RoF) and diameter of fibers (DoF). BBD of three levels (lowest value = -1; middle value = 0 and highest value = 1) for three variables or factors x_1 = work distance (Wd), x_2 = feed rate (Fr), and x_3 = air pressure (Ap). Fifteen experiments were run, three of these correspond to the central design point (PSF13-15) and twelve to the extremes of BBD (PSF1-12). Table 1 shows experiments codes, levels associated to each variable and the corresponding values of the variables.

Table 1

From the mathematical models obtained from the response surface regression it is possible to obtain the desirability (d_i) functions necessary to find the combination of variables to simultaneously satisfy two conditions: I) maximum ratio of fibers (RoF) and II) minimum diameter of fibers (DoF).

Desirability always takes values between 0 and 1, where $d_i = 0$ would mean an undesirable response, and $d_i = 1$ a completely desirable response.[33] All statistical analyses were done with STATGRAPHICS Centurion XVI software (version 16.1.11).

From the desirability function, three different morphologies were taken, i) a morphology with the highest ratio of fibers (RoF) and the smallest diameter of fibers (DoF) (desirability = 1); ii) a morphology with the lowest RoF and the highest DoF (desirability = 0) and iii) an intermediate result with a desirability value of 0.45.

2.5. Roughness measurements

Roughness at microscale was measured using an optical profilometer Olympus DSX500. The roughness parameter obtained was the arithmetic mean height, R_a, using a calculated cut-off (λ_c) based in the standard UNE EN ISO 4288.[34]

2.6. Contact Angle measurements

Contact angle measurements were performed using an OCA-15 KRÜSS GmbH tensiometer based on the drop method. The contact angle for two testing liquids (distilled, deionized water and glycerol) was obtained from the average of fifteen drops of 3 μL, five drops in different locations (ensuring at least a minimum distance between drops of 2 mm) of the same surface of three different specimens. All contact angle measurements were carried out at room temperature (22-24ºC) and at 35% of relative humidity.

3. Results and discussion

Polysulfone concentration of 10% was selected because this concentration is in the limit of chains entanglement to produce structures constituted by fibers and microbeads,[3,35] leading to a microstructure usually called beads-on-string morphology.[15]

As an example, Figure 2 shows two typical SEM images of PSf materials obtained by SBS. In general, two main micro-constituents can be observed, material accumulations in the form of pearls or corpuscles and fibers confirming the beads-on-string morphology. Generally, the appearance of pearls is justified in terms of the

concentration of the solution to be blow spun.[27,36] When this concentration is low enough some individual drops can be ejected from the nozzle without being stressed as to get real fibers.

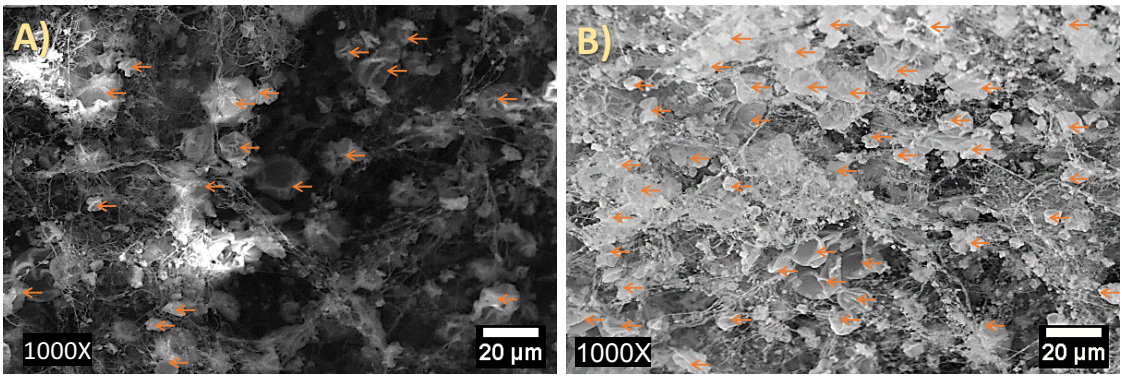

Figure 2. SEM micrographs of PSF fibers fabricated by SBS: A) sample with maximum RoF (sample PSF-10) and B) sample with minimum RoF (sample PSF-6).

Among the SBS conditions considered in this work, different beads-on-string morphologies were obtained which are characterized by having different relative amount of fibers with larger or smaller diameters. In order to have visual information about the extremes in terms of relative amount of fibers Figure 2A and 2B show SEM images of the samples with the highest and lowest ratios of fibers respectively. Although some morphological characteristics might be explained by the possible previous presence of solvent traces, FTIR spectra did not show any evidence of them. Besides, under similar SBS conditions of the present work and using solutions of other polymers with acetone based mixtures or other solvents of similar boiling points, traces of solvents in the final materials were not detected by FTIR (characteristic bands) or TGA (weight losses at temperatures in the range 40-100 ºC) or DSC (endothermic peaks at around 50-60 ºC) at least within the sensibility of the equipments.[33,37,38]

After making the corresponding image analysis, values of ratio of fibers, RoF, were obtained for all the samples prepared under the different SBS conditions (Table 2).

Table 2

It can be observed that SBS conditions clearly affect the RoF showing maximum difference between samples 6 and 10 with a relative change higher than 65%. For these two samples the feed rate used was the same, however, the other two processing conditions or factors were different. Therefore, it is difficult, even qualitatively, to predict the main factor inducing a particular morphology since a complex combination of both factors may be the main cause of morphological changes. Hence, a deeper analysis based on statistics should be done. However, in general, this kind of studies requires many data arising from multiple experiments.

Box-Behnken surface methodology, BBD, is a statistical method which main goal is to reduce the number of experiments, without decreasing precision in comparison with other methods of factorial planning.[39] BBD uses the analysis of variance to obtain a quadratic model, Equation (2), where γ is the response variable, β is the regression coefficient of the model, x is the independent variable and ε is the random error component. By the use of the quadratic model the effect of factors and their combinations on a particular response (for instance, RoF) can be visualized in the so-called Pareto chart (Figure 3A). In this diagram it is possible to arrange factors and combination of factor in terms of priority respect to their influence on the responses studied. Besides, it is also possible to make other kind of evaluations by the use of lineal (Figure 3B) or surface (Figure 3C-E) response plots if individual or combined contributions are wanted to be analyzed.

$$\gamma = \beta_0 + \sum_{i=1}^{k} \beta_i x_i + \sum_{i=1}^{k} \beta_{ii} x_i^2 + \sum \sum_{i<j=2}^{k} \beta_{ij} x_i x_j + \varepsilon \qquad (2)$$

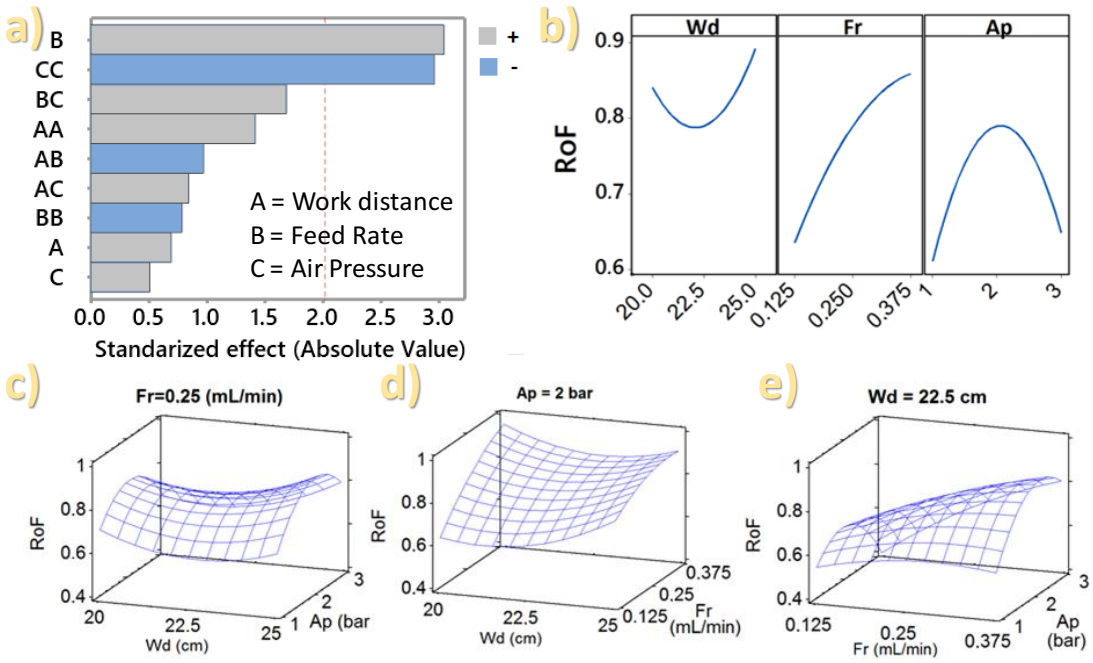

Figure 3. Influence of factors, X, and combination of factors, XX (where X are A=work distance, B=Feed rate and C=Air pressure) on RoF, a) Pareto chart showing standardized effect; b) lineal plot of independent variables and response surface diagrams of combined effects; c) working distance and Air pressure; d) working distance and feed rate, and e) feed rate and air pressure.

The analysis of variance gave a coefficient of determination, $R^2 = 0.8408$, indicating the model was good enough with 84% of assertiveness. Therefore, the model can make predictions in the particular case of preparing PSf based materials by SBS. The lack of significant fitting obtained, p, was 0.011, which points out a very low error in the predictions made by the use of Equation (3).

$$\gamma_1 = 5.94 - 0.538x_1 + 4.51x_2 + 0.089x_3 + 0.0123x_1^2 - 2.73x_2^2 - 0.1603x_3^2 - 0.162[x_1][x_2] + 0.0176[x_1][x_3] + 0.702[x_2][x_3] \quad (3)$$

According to the Pareto chart (Figure 3A), feed rate (B) and quadratic air pressure (CC) have a higher impact (higher estimated standardized effect) on the formation of fibers. While feed rate (B) has a positive influence, the quadratic air pressure (CC) has a negative effect. Therefore, a balance between these two factors should be taken into

account in order to obtain a higher ratio of fibers, something that had already been reported.[27]

Figure 3B shows the tendencies predicted by Equation (3) for the response γ_1 = RoF as a function (in an independent way) of the factors Wd, Fr and Ap. In the particular case of Ap an open down parabolic tendency is observed, being in accordance with other results obtained for other systems.[40,41] In fact, maintaining Ap at a medium level (2 bar) the RoF increases. Probably, low air pressures (1 bar) does not allow effectively evaporating the solvent leading to the formation of a drop at the end of the capillary or the nozzle exit. If the size of this drop is large enough the pressure exerted by the air might be only used to take out the drop but not to stretch it in the form of fibers thus reaching the material the collector in the form of small pearls or agglomerates. On the other hand, if high air pressure is used, fast solvent evaporation can occur leading also to solid material lumps before fibers formation. Furthermore, RoF tends to increase as Fr increases while, when Wd is considered as the experimental factor RoF respond has an open up parabolic tendency; however, the variation is very small suggesting a poor influence of Wd on RoF.

Three dimensional (3D) response surface plots have been considered to better understand the interactions between factors on a particular effect or response.[42-44] Figures 3C-E show, in terms of a 3D plot based on the model Equation (3), combined effects of factors on RoF.

Figure 3C shows the work distance and Air pressure combined influence on RoF showing again quadratic functions for both factors with more air pressure influence on

the RoF. On the other hand, as can be seen in Figure 3D the effect of Fr is enhanced at lower working distances. Finally, the other factor, the Ap should be medium to favor the effect of Fr on the relative amount of PSF fibers formed by SBS (Figure 3E).

Figure 4 shows representative SEM images corresponding to samples of blow spun PSf with the highest difference in terms of fiber sizes. As can be seen, a similar morphology is obtained. Therefore, in order to find differences deeper analysis should be done. When the diameter of fibers is chosen as the parameter of analysis, the average value is usually used.[43,45-48] However, techniques to produce fibers such as melt blowing,[49] electrospinning[50] and centrifugal spinning[51] lead to more or less complex fiber distributions that may depend on the experimental conditions and mainly on the material. Therefore, more than the simple calculation of the arithmetic mean value, the identification of the kind of distribution is necessary since, in addition to the mean size, the heterogeneity of fiber sizes might play a very important role on the final properties the material. Anderson-Darling statistic (ADs) is usually a good way to identify different kinds of distributions. ADs is used to test the goodness of a certain distribution function used to fit the distribution of values associated to a sample population of size *n*.

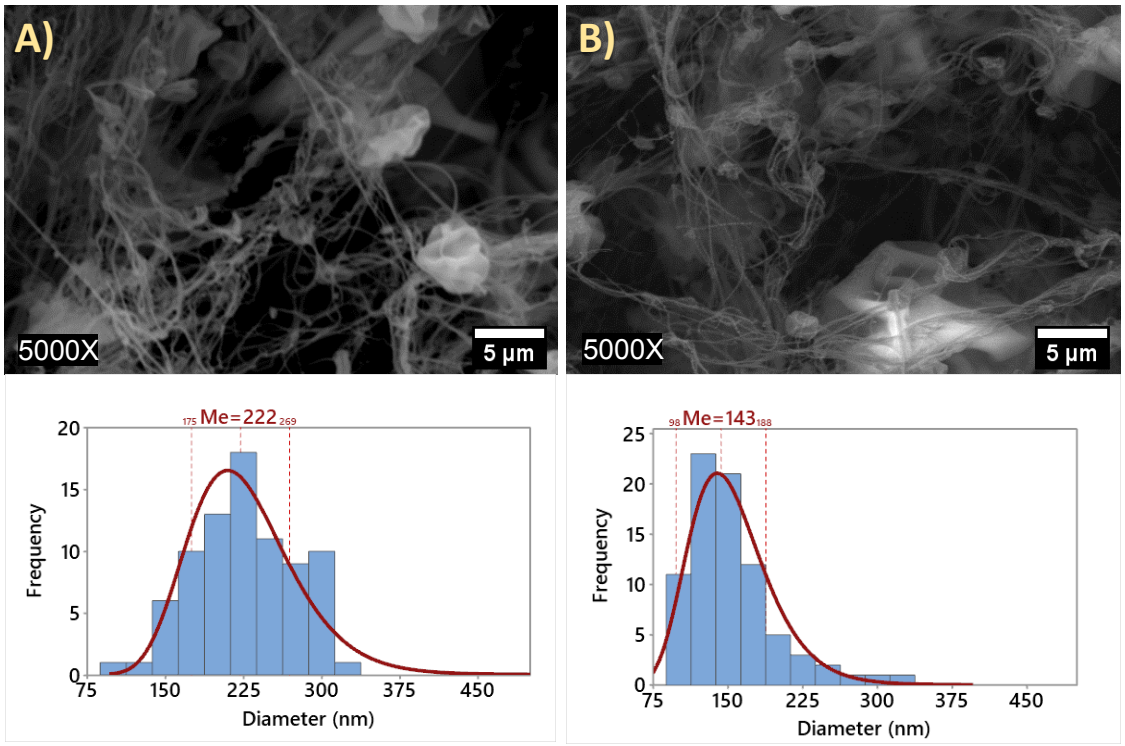

Figure 4. SEM micrographs of PSf fibers fabricated by SBS: A) maximum values of DoF (sample PSF-9), B) minimum values of DoF (sample PSF-10). Standard deviations are pointed out by dashed lines.

Applying ADs to the data of fibers diameters it is necessary to consider the null hypothesis (Ho) that assumes DoF obtained can be fitted by a specific distribution function, while the alternative hypothesis (Ha) suggests that diameters of the fibers cannot be fitted by a specific distribution function. Table 3 shows the acceptance or rejection of null hypothesis for normal, lognormal, Weibull and Gamma distribution with a level of statistical significance of 95%, rejecting Ho if the calculated P-value (probability of certainty) is equal or less than 0.05.[52]

Table 3

As can be concluded from Table 3, Anderson-Darling statistical indicates DoF experimental data can be well fitted by lognormal and gamma distributions. Although the gamma distribution has a good acceptance (87%), the lognormal distribution can be

accepted in all the experiments, resulting therefore the best distribution function to fit the experimental data and improve subsequent statistical treatments.

Lognormal distribution is not a symmetric distribution therefore; study of average is not significant for treatment of data, so median DoF value (Table 2) was used for robust fitting due this value is not affected by extreme.

Diameter of fibers (DoF), other morphological response, was also evaluated using the same method. In particular, the same statistical treatment based on Box-Behnken surface methodology was used but using the median value as input with a level of significance of 10% (x = 0.1). Therefore, a quadratic model for DoF, Equation (4), was also obtained by the analysis of variance, residual analysis indicates there is not evidence of lack of significant fitting (p value = 0.0213 and R^2 = 73.24).

$$\gamma_2 = 602 - 8.5x_1 - 1667x_2 - 101x_3 - 0.32x_1^2 + 3x_2^2 + 26.2x_3^2 + 79.3[x_1][x_2] + 0.67[x_1][x_3] - 80.2[x_2][x_3] \quad (4)$$

According to Pareto chart, the highest influence on the DoF was found for the quadratic air pressure coefficient (CC) and the combined coefficient due to effect of working distance and feed rate (AB), indicating these terms have higher contribution for the prediction of DoF. As a conclusion, it should be necessary to find the balance between these coefficients in order to decrease DoF. However, negatives coefficients as the independents terms Fr and Wd, interaction between Fr and Ap, and quadratic Wd point out that modification of individual coefficient, just in one way, could cause a break in the balance between factors affecting negatively DoF (Figure 5A).

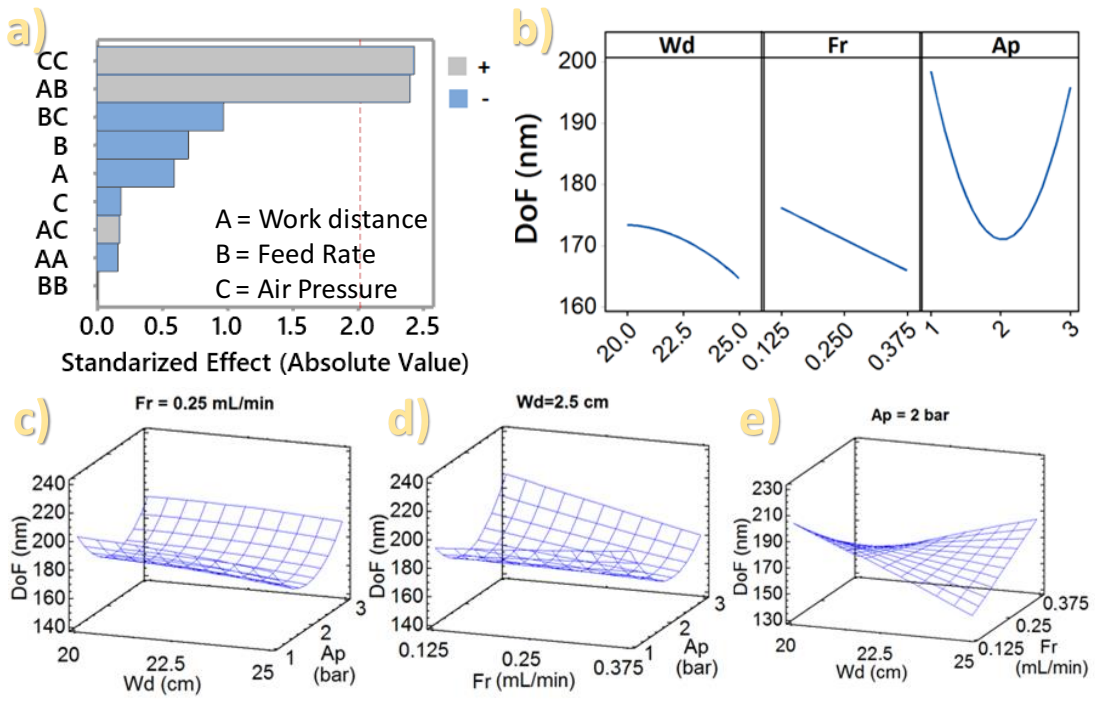

Figure 5. Influence of factors, X, and combination of factors, XX on DoF: a) Pareto chart showing standardized effect; b) lineal plot of independent variables and response surface diagrams due to combined effects: c) working distance and air pressure; d) feed rate and air pressure and e) working distance and feed rate.

Figure 5B shows the effects of individual factors (Wd, Ap, and Fr) on DoF calculated from Equation (4). Particularly, Ap presented an open up parabolic tendency indicating this factor affects directly the DoF, similar to that reported for other polymeric systems.[53] Although parabolic profile of DoF as a function of Ap is contrary to that one observed for the RoF (DoF: from decreasing to increasing and RoF: from increasing to decreasing) in both cases an intermediate Ap value separates the change of tendency. Besides, neither working distance nor feed rate have an important effect separately. Although they show a tendency to decrease DoF as they increase, their influence is smaller than even the statistical significance, therefore, those factors individually considered were discarded. On the other hand, the combined effects arising from two factors were evaluated by 3D surface response plots, keeping a middle value for the factor not considered in the combined effect (Figure 5C, E and D). It is observed that

the Ap is always the higher contribution to the combined effects on the DoF response (Figure 5 C and D). Furthermore, the effect arising from the combination of Fr and Wd is very low (Figure 5 D). In terms of Wd effect on the DoF it seems that fibers of polysulfone observed are already formed at least during the first 20 cm of flying because there are not important changes of shape and size at longer working distances. On the other hand, considering the effect of Ap combined with feed rate it could be said that production of fibers, at least in the range 0.125 - 0.375 mL/min, is not altered in terms of DoF. This result can be explained considering that the speed of liquid ejection from the nozzle is slow or fast enough as to have not influence on the stretching action exerted by the air pressure, being in accordance with that reported for PEO produced by SBS.[42]

Maintaining the Ap constant the combine effect exerted by Wd and Fr factors lead to the small diameter of fibers when the working distance is the longest and the Fr is the lowest. A possible explanation may be to consider a slower evaporation rate at the nozzle exit allowing higher ability for the solution to be stretched, leading therefore to fiber with small diameters.

Up to now, Box-Behnken response surface methodology has been applied to understand the influence of different SBS conditions on RoF and DoF separately. However, to obtain a specific morphology in terms of all its features it should be necessary to find the best experimental conditions (factors) within optimal ranges, leading to a certain degree of compliance respect to the proposed criteria for each variable or response. One of the most used methods in industry dealing with the optimization of multiple response processes is the desirability function approach.[54]

Considering there are two responses, desirability function approach transforms an estimated response obtained by a regression equation (for example, γ_1 and γ_2 would be the estimated values of Rof and DoF factors obtained from Equation 3 and 4 respectively) into a scale-free value, called desirability, d_i.[55,56] Then, the overall desirability function, D, is defined as the geometric mean of the individual desirability functions of each response, Equation (5), which will be maximized or minimized, respectively.[57]

$$D = \left(\prod_{i=1}^{n} d_i(\gamma_i)\right)^{\frac{1}{n}} \quad (5)$$

where $d_i(\gamma_i)$ is the individual desirability functions of each response, γ_i, and n the number of responses.

In order to find the values of the factor that allow determining a specific morphology from desirability function, 3D plots of desirability as a function of two factors (Figure 6) and estimated experimental SBS conditions from particular values of desirability (Table 4) are used. From the three plots of Figure 6 it can be concluded that, for this system, a desirability value closer to 1 is found when it is used a middle value of air pressure (2 bars), the lowest value of Wd (20 cm), and the higher value of Fr (0.375 mL/min).

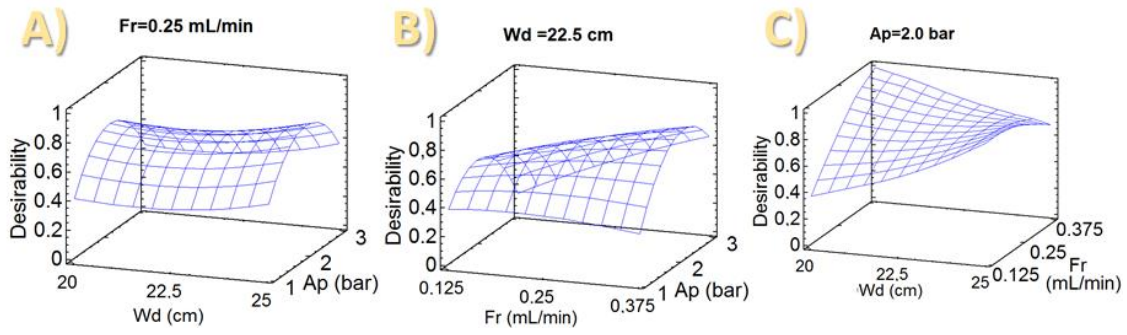

Figure 6. 3D plots of desirability as a function of two factors: A) Wd and Ap, B) Fr and Ap, and C) Wd and Fr.

Table 4

As can be seen in Table 4, the optimal SBS conditions to obtain the highest ratio of fibers and the small diameter of them (when the desirability is equal to 1) were estimated: work distance = 20 cm, feed rate = 0.375 mL/min and air pressure = 2.2 bars. In order to corroborate that the estimated experimental conditions actually lead to the expected or estimated optimal responses, RoF = 96.5 % and Dof = 141 nm (Table 4), polysulfone materials were prepared in the laboratory using those experimental conditions.

Figure 7 shows a representative SEM image of the PSf sample obtained using the estimated optimal SBS conditions (Figure 7A) and the corresponding bar distribution diagram of DoF (Figure 7B) obtained from the analysis of three images like that one of Figure 7A. Besides, from the analysis of SEM images the experimental value of RoF was also obtained. As can be seen, there is a high coincidence between the estimated values and the experimental ones (see the inserted table in Figure 7B).

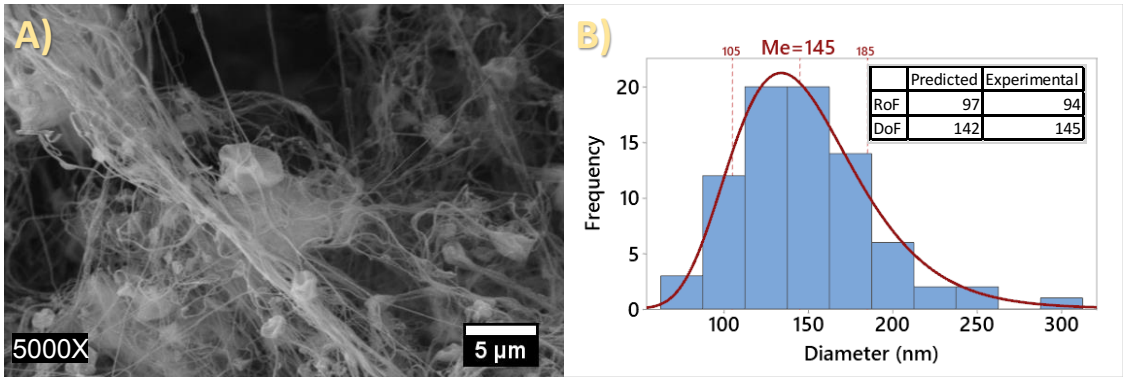

Figure 7. Representative SEM image of PSF sample obtained using the estimated optimal SBS conditions (A) and histogram of DoF (B). Standard deviations are pointed out by dashed lines.

All these results point out that the use the desirability function approach is a very easy an effective method to estimate the best solution blow spinning conditions to prepare Polysulfone based materials with a particular morphology. According to the desirability values, the conditions represented by desirability values of 1, 0.46 and 0.15 (Table 4) were used to prepare samples named as optimal, medium and non-optimal respectively. Where optimal sample, OS, is characterized by having the highest RoF and lowest DoF, non-optimal sample, NS, is characterized by having the lowest RoF and highest DoF and medium sample, MS, is characterized by a morphology having middle values of RoF and DoF respectivly.

Up to now, it has been demonstrated therefore that multi-response optimization based on desirability value is useful to control surface morphology of polysulfone, because it allows choosing the proper SBS processing conditions. Taking into account that topography greatly influences wettability behavior of materials it is time now to see if, just tuning the SBS conditions, control of polysulfone wettability behavior is possible.

Several works showed how polysulfone surfaces can condition the contact angle formed between a water drop and the polymer surface. For instance, E. Bormashenko et al. showed that the contact angle of water on a flat smooth surface of extruded PSf is 79º,[58] on the other hand, PSf based materials made of electrospun fibers with average diameter of about 800 nm presented a water contact angle of 103.8º.[59] These results agree the well known influence of surface morphology on the contact angle of a liquid. In general, it is satisfied that surface heterogeneity powers physicochemical properties of the material surface.[60] In other words, if a surface is chemically hydrophobic it will behave even more hydrophobic if its roughness increases and vice versa. In fact, J. Teno

obtained even higher water contact angles than those obtained in references [58,59] in more complex PSf surfaces obtained by SBS using a commercial airbrush, 107º.[23]

In the present work contact angle measurements, using two testing liquids, were carried out on three of the samples prepared by SBS covering a wide range in terms of different topographies (Table 5).

As can be seen contact angles (Table 5) are very high indicating a clear hydrophobic behavior of the PSf. Besides, in the case of the sample BS-6 the behavior is even superhydrophobic since a water contact angle value of 150º is clearly overcome. There are two states or models usually used to describe the wettability behavior of solid surfaces Wenzel[60] and Cassie-Baxter[2] models respectively. In the Wenzel's model, there is a relation between the real contact angle formed on the rough surface, θ_W, and the contact angle formed on a perfectly smooth surface, θ

$$\cos\theta_W = r \cdot \cos\theta \qquad (6)$$

Where r is the so called roughness factor.[60] Taking into account a value of about 80º for the water contact angle when the water drop is deposited on a smooth surface of PSf[58,59] and the roughness measurements for the samples under study, an estimation of the real contact angle could be done. In Table 6 the arithmetical mean roughness, R_a, and the roughness factor, r, of the three samples chosen are gathered. As can be seen, although differences in roughness are evident, the roughness factor does not depend on the samples under study and therefore the estimated water contact angle, θ_W, using Equation (6), does not depend on the kind of sample either (Table 5). Although all these estimated contact angles are higher than 80º, they are not high enough as to adequately predict the real values experimentally obtained (Table 5). A possible reason of that

wrong prediction by defect might be that the real surface in contact with the liquid is higher than that considered from the optical profilometer measurements. In fact, with the profilometer, a measurement at microscale is taken into account; however, the topographic features, which seems to be the main cause of changes in the wettability behavior (fibers and beads), have submicrometric dimensions.

Table 5

The parameter R_a provides information about the mean heterogeneities of the surface rather than the increase of surface due to the roughness itself. As can be seen, comparison between the values of contact angles in Table 5 with R_a values in Table 6 points out a better correlation between surface heterogeneity and wettability. However, again the scale factor should be taken into account. As consequence, the Cassie-Baxter approximation seems to be more adequate to justify our experimental results.

Table 6

In the Cassie-Baxter approximation,[61] the relation between the real contact angle formed on the rough surface, θ_{CB}, and the contact angle formed on the smooth surface, θ, is given by

$$\cos\theta_{CB} = \varphi_S \cdot \cos\theta + \varphi_S - 1 \qquad (7)$$

Where φ_S is the fraction of solid surface in direct contact with the liquid. Taking into account a value of about 80º for the water contact angle when the water drop is deposited on a perfectly smooth surface[58,59] and the experimental value of the contact angle on the rough surfaces, the fraction of solid surface in contact with the liquid, φ_S, could be estimated from Equation (7). Then, with this estimated fraction, φ_S, for a particular microscopic region of observation, knowing the distribution of fibers sizes in terms of their diameters and the relative amount of fibers in terms of RoF, it would be possible to make an estimation of the number of fibers and beads or solid material in

form of fibers and beads that will be in contact with a water drop. This estimation can be even schematically drawn leading to a theoretical morphology for a particular contact angle. The estimated and real morphologies of the three samples under consideration are shown in Figure 8. As can be seen, the estimated morphologies are quite good qualitative predictions of the real morphologies. Therefore, the Cassie-Baxter model seems to be a very good model to explain the wettability behavior of the SBS PSf materials prepared in the present work.

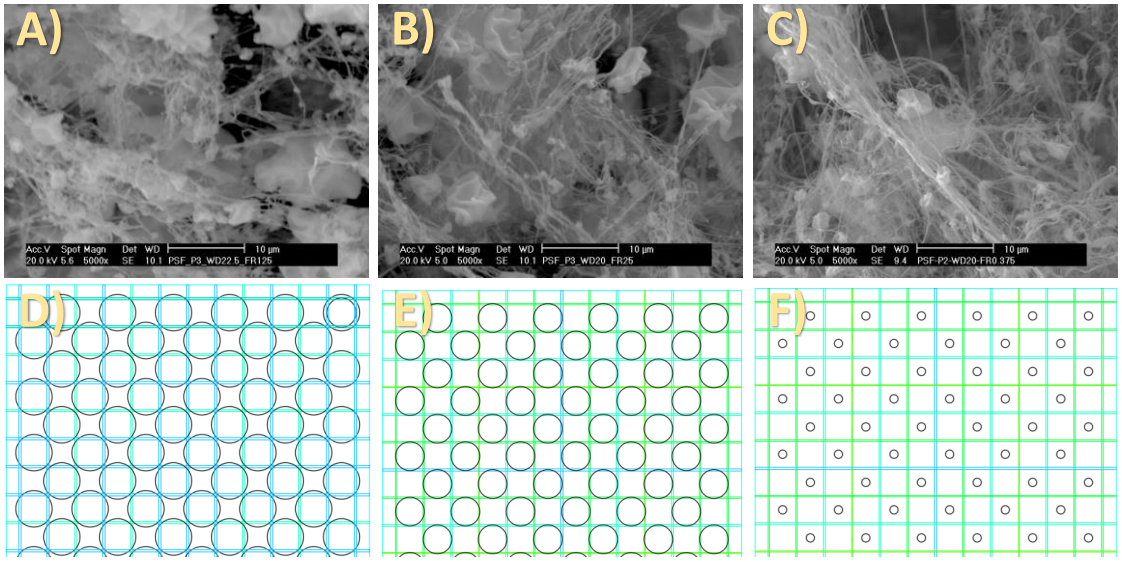

Figure 8. Real images obtained by SEM representing the morphology of the samples a) PSF-6; b) PSF-2 and c) PSF-11 and estimated morphologies from the Cassie-Baxter model of the samples d) PSF-6; e) PSF-2 and f) PSF-11.

As can be seen, the higher water contact angle is formed on the surface constituted by thicker fibers but less amount of them. This result may be interpreted considering that, up to the limit of surface tension, the smaller morphological features (fibers diameters) the higher the solid surface available for the liquid drop and consequently the lower contact angle. This result actually is in accordance with the geometrical evidence of having higher surface area, a particular amount of material constituted by smaller particles. In general, when materials are constituted only by fibers it is possible to attain higher water contact angles for thinner fibers. However, it seems that when a combined

microstructure is obtained, constituted by fibers and beads, different conclusion can be extracted. Water contact angle will depend on the fraction of air in contact with the liquid that, in turn, should depend on the whole microstructure, in other words, a particular combination of microconstituents, their shapes and their sizes.

4. Conclusion

In this work it was shown that solution blow spinning, SBS, is a good method to prepare polysulfone based materials, PSf, with controlled morphology. Besides, Box-Behnken response surface methodology was demonstrated to be useful to understand the effects of SBS conditions (working distance, feed rate and air pressure) on a couple of morphological characteristics of the materials prepared. In particular, feed rate and air pressure had the highest effect on the relative amount of fibers produced while air pressure and a particular balance between working distance and feed rate had the highest impact on the size of fibers. On the other hand, it was demonstrated that the use of the desirability function approach is a very easy an effective method to estimate the best solution blow spinning conditions to prepare polysulfone based materials with a specific morphology. The superhydrophobic behavior of SBS PSf prepared in this work could be better described by the Cassie-Baster model. It was demonstrated the possibility of designing a material with a wettability behavior induced by a tailored morphology, which, in turn, can be obtained from SBS processing conditions provided using the Box-Behnken method and desirability function approach.

Acknowledgments

Fondos de Investigación de Fco. Javier González Benito, política de reinversión de costes generales, Universidad Carlos III de Madrid [2012/00130/004] and Acción Estratégica en Materiales Compuestos Poliméricos e Interfases, Universidad Carlos III

de Madrid [2011/00287/002]. Besides, authors greatly appreciate the Consejo Nacional de Ciencia y Tecnología (CONACyT-México) for financial support associated to a the scholarship number 625396.

Keywords: Solution blow spinning; polysulfone; morphology; Superhydrophobic, Wettability.

5. References

[1] V. Belaud, S. Valette, G. Stremsdoerfer, M. Bigerelle, S. Benayoun, *Tribol. Int.* **2015**, *82*, 343.

[2] A.B.D. Cassie, S. Baxter, *Trans. Faraday Soc.* **1944**, *40*, 546.

[3] M. Al-Qadhi, N. Merah, A. Matin, N. Abu-Dheir, M. Khaled, K. Youcef-Toumi, *J. Polym. Res.* **2015**, *22*, 207.

[4] W.E. Teo, S. Ramakrishna, *Nanotechnology* **2006**, *17*, 89.

[5] S.S. Ramkumar, C. Roedel, J. *Appl. Polym. Sci.* **2003**, *9*, 3626.

[6] E. Stojanovska, E. Canbay, E.S. Pampal, M.D. Calisir, O. Agma, Y. Polat, R. Simsek, N.A.S. Gundogdu, Y. Akgul, A. Kilic, *RSC Adv.* **2016**, *6*, 83783.

[7] V.I. Tkatch, A.I. Limanovskii, S.N. Denisenko, S.G. Rassolov, *Mater. Sci. Eng. A* **2002**, *323*, 91.

[8] L. Zhang, P. Kopperstad, M. West, N. Hedin, H. Fong, *J. Appl. Polym. Sci.* **2009**, 114, 3479.

[9] B. Vazquez, H. Vasquez, K. Lozano, *Polym. Eng. Sci.* **2012**, *5*, 2260.

[10] Zhang, D. Dry spinning of synthetic polymer fibers. *Advances in filament yarn spinning of textiles and polymers*. **2014**, 187.

[11] A. Greiner, J.H. Wendorff, *Angew. Chemie* **2007**, *46*, 5670.

[12] E.S. Medeiros, G.M. Glenn, A.P. Klamczynski, W.J. Orts, L.H.C. Mattoso, *J. Appl. Polym. Sci.* **2009**, *113*, 2322.

[13] L. Li, W. Kang, X. Zhuang, J. Shi, Y. Zhao, B. Cheng, *Mater. Lett.* **2015**, *160*, 533.

[14] J.E. Oliveira, L.H.C. Mattoso, W.J. Orts, E.S. Medeiros, *Adv. Mater. Sci. Eng.* **2013**, 409572.

[15] J.L. Daristotle, A.M. Behrens, A.D. Sandler, P. Kofinas, *ACS Appl. Mater. Interfaces* **2016**, *8*, 34951.

[16] Y. Polat, E.S. Pampal, E. Stojanovska, R. Simsek, A. Hassanin, A. Kilic, A. Demir, A.Yilmaz, *J. Appl. Polym. Sci.* **2016**, *133*, 43025.

[17] M. Wang, C.Y. Yue, B. Chua, *J. Mater. Sci. Mater. Med.* **2001**, *12*, 821.

[18] I. Shabani, V. Haddadi-Asl, M. Soleimani, E. Seyedjafari, S.M. Hashemi, *ACS Appl. Mater. Interfaces* **2014**, *6*, 72.

[19] B.D. Ratner, A.S. Hoffman, F.J. Schoen, J.E. Lemons, *Biomaterials Science: An Introduction to Materials in Medicine*, Academic Press, **2004**.

[20] S.K. Bowry, *International Journal of Artificial Organs* **2002**, *25*, 447.

[21] X.Y. Yuan, Y.Y. Zhang, C. Dong, J. Sheng, *Polym. Int.* **2004**, *53*, 1704.

[22] Y. Yao, P. Zhu, H. Ye, A. Niu, X. Gao, D. Wu, *Front. Chem. China* **2006**, *1*, 334.

[23] J. Teno, G. González-Gaitano, J. González-Benito, *J. Polym. Sci. Part B Polym. Phys.* **2017**, *55*, 1575.

[24] S. Ö. Gönen, M. Erol Taygun, S. Küçükbayrak, *Mater. Sci. Eng. C* **2016**, *58*, 709.

[25] R.E. Bruns, I. Scarminio, B. Barros Neto, *Statistical Design – Chemometrics*, Elsevier Science, **2006**.

[26] C. Bilbao-Sainz, B. Sen Chiou, D. Valenzuela-Medina, W.X. Du, K.S. Gregorski, T.G. Williams, D.F. Wood, G.M. Glenn, W.J. Orts, *Eur. Polym. J.* **2014**, *54*, 1.

[27] J.E. Oliveira, E.A. Moraes, R.G.F. Costa, A.S. Afonso, L.H.C. Mattoso, W.J. Orts, E.S. Medeiros, *J. Appl. Polym. Sci.* **2011**, *122*, 3396.

[28] F. Liu, R.J. Avena-Bustillos, R. Woods, B. Den Chiou, T.G. Williams, D.F. Wood, C. Bilbao-Sainz, W. Yokoyama, G.M. Glenn, T.H. McHugh, F.J. Zhong, *J. Food Sci.* **2016**, *1*, 3015.

[29] P.W. Araujo, R.G. Brereton, *TrAC - Trends Anal. Chem.* **1996**, *5*, 156.

[30] N.R. Costa, J. Lourenço, Z.L. Pereira, *Chemom. Intell. Lab. Syst.* **2011**, *107*, 234.

[31] C. Cojocaru, P.P. Dorneanu, A. Airinei, N. Olaru, P. Samoila, A. Rotaru, *J. Taiwan Inst. Chem. Eng.* **2017**, *70*, 267.

[32] A. Rabbi, K. Nasouri, H. Bahrambeygi, A.M. Shoushtari, M.R. Babaei, *Fibers Polym.* **2012**, *13*, 1007.

[33] J. Teno, A. Corral, G. Gorrasi, A. Sorrentino, J. González-Benito, *Mater. Today Commun.* **2019**, *20*, 100581.

[34] L. Vera Candioti, M.M. De Zan, M.S. Cámara, H.C. Goicoechea, *Talanta* **2014**, *124*, 123.

[35] K.H. Chang, H.L. Lin, *J. Polym. Res.* **2009**, *16*, 611.

[36] J. Oliveira, G.S. Brichi, J.M. Marconcini, L.H.C. Mattoso, G.M. Glenn, E.S. Medeiros, *J. Eng. Fiber. Fabr.* **2014**, *9*, 117.

[37] M. Iorio, J. Teno, M. Nicolás, R. García-González, V. H. Peláez, G. González-Gaitano, J. González-Benito, *Colloid Polym. Sci.* **2018**, *296*, 461.

[38] J.E. Oliveira, E.A. Moraes, J.M. Marconcini, L.H.C. Mattoso, H.C. Luiz, G.M. Glenn, E.S. Medeiros, *J. Appl. Polym. Sci.* **2013**, *129*, 3672.

[39] R.H. Myers, D.C. Montgomery, G. Geoffrey Vining, C.M. Borror, S.M. Kowalski, *J. Qual. Technol.* **2004**, *36*, 53.

[40] M. Khajeh, *J. Supercrit. Fluids* **2011**, *55*, 944.

[41] L. Li, W. Kang, Y. Zhao, Y. Li, J. Shi, B. Cheng, *Ceram. Int.* **2014**, *41*, 409.

[42] H. Lou, W. Li, C. Li, X. Wang, *J. Appl. Polym. Sci.* **2013**, *130*, 1383.

[43] D.D. da Silva Parize, M.M. Foschini, J.E. de Oliveira, A.P. Klamczynski, G.M. Glenn, J.M. Marconcini, L.H.C. Mattoso, *J. Mater. Sci.*, **2016**, *51*, 4627.

[44] D. Tang, X. Zhuang, C. Zhang, B. Cheng, X. Li, *J. Appl. Polym. Sci.* **2015**, *132*, 42326.

[45] M. Vural, A.M. Behrens, O.B. Ayyub, J.J. Ayoub, P. Kofinas, *ACS Nano* **2015**, *9*, 336.

[46] M. Gonzalez-Abrego, A. Hernandez-Granados, C. Guerrero-Bermea, A. Martinez de la Cruz, D. Garcia-Gutierrez, S. Sepulveda-Guzman, R. Cruz-Silva, *J. Sol-Gel Sci. Technol.* **2017**, *81*, 468.

[47] R.G.F. Costa, G.S. Brichi, C. Ribeiro, L.H.C. Mattoso, *Polym. Bull.* **2016**, *73*, 1.

[48] S. Srinivasan, S.S. Chhatre, J.M. Mabry, R.E. Cohen, G.H. McKinley, *Polymer* **2011**, *52*, 3209.

[49] C.J. Ellison, A. Phatak, D.W. Giles, C.W. Macosko, F.S. Bates, *Polymer* **2007**, *48*, 3306.

[50] O.O. Dosunmu, G.G. Chase, W. Kataphinan, D.H. Reneker, *Nanotechnology* **2006**, *17*, 1123.

[51] Y. Fang, A.R. Dulaney, J. Gadley, J. Maia, C.J. Ellison, *Polymer* **2016**, *88*, 102.

[52] T.W. Anderson, D.A. Darling, *J. Am. Stat. Assoc.* **1954**, *49*, 765.

[53] R. Vasireddi, J. Kruse, M. Vakili, S. Kulkarni, T.F. Keller, D.C.F. Monteiro, M, Trebbin, *Sci. Rep.* **2019**, *9*, 14297.

[54] D.J. Neubauer, *Qual. Technol.* **2008**, *40*, 348.

[55] I.J. Jeong, K.J. Kim, *Eur. J. Oper. Res.* **2009**, *195*, 412.

[56] G. Derringer, R. Suich, *J. Qual. Technol.* **2018**, *12*, 214.

[57] R. Amdoun, L. Khelifi, M. Khelifi-Slaoui, S. Amroune, M. Asch, C. Assaf-Ducrocq, E. Gontier, *Iran. J. Biotechnol.* **2018**, *6*, 11.

[58] E. Bormashenko, R. Pogreb, G. Whyman, Y. Bormashenko, R. Jager, T. Stein, A. Schechter, D. Aurbach, *Langmuir* **2008**, *24*, 5977.

[59] P.P. Dorneanu, A. Airinei, M. Homocianu, N. Olaru, *Mater. Res. Bull.* **2015**, *64*, 306.

[60] R.N. Wenzel, *Ind. Eng. Chem.* **1936**, *28*, 988.

[61] M.S. Bell, A. Shahraz, K.A. Fichthorn, A. Borhan, *Langmuir* **2015**, *31*, 6752.

Tables

Table 1. Experiment codes for the levels and factors considered when applying the BBD.

Run	Sample code	(x_1)	(x_2)	(x_3)	Work distance (cm)	Feed rate (mL/min)	Air pressure (bar)
1	PSF-1	-1	0	-1	20	0.25	1
2	PSF-2	-1	0	1	20	0.25	3
3	PSF-3	1	0	-1	25	0.25	1
4	PSF-4	1	0	1	25	0.25	3
5	PSF-5	0	-1	-1	22.5	0.125	1
6	PSF-6	0	-1	1	22.5	0.125	3
7	PSF-7	0	1	-1	22.5	0.375	1
8	PSF-8	0	1	1	22.5	0.375	3
9	PSF-9	-1	-1	0	20	0.125	2
10	PSF-10	1	-1	0	25	0.125	2
11	PSF-11	-1	1	0	20	0.375	2
12	PSF-12	1	1	0	25	0.375	2
13	PSF-13	0	0	0	22.5	0.25	2
14	PSF-14	0	0	0	22.5	0.25	2
15	PSF-15	0	0	0	22.5	0.25	2

Table 2. Ratio of fibers, RoF, average diameter of fibers, DoF, standard deviation for the diameters of fibers, σ, and median of the fibers diameters, Me.

Sample Code	RoF (%)	DoF (nm)	σ (nm)	Me(nm)
PSF-1	71	198	57	199
PSF-2	70	185	52	179
PSF-3	63	218	54	208
PSF-4	79	199	43	195
PSF-5	49	178	42	178
PSF-6	31	218	56	210
PSF-7	69	214	52	205
PSF-8	86	200	44	196
PSF-9	69	226	47	222
PSF-10	89	154	45	143
PSF-11	86	149	40	146
PSF-12	86	174	42	166
PSF-13	80	183	59	171
PSF-14	77	195	63	183
PSF-15	80	169	49	158

Table 3. Distribution fitting analysis: A = accepted and R = Rejected.

	Normal		Lognormal		Weibull		Gamma	
Sample Code	P-Value	A/R	P-Value	A/R	P-Value	A/R	P-Value	A/R
PSF-1	0.004	R	0.117	A	<0.01	R	0.139	A
PSF-2	0.023	R	0.131	A	<0.01	R	0.148	A
PSF-3	0.002	R	0.449	A	<0.01	R	0.189	A
PSF-4	0.000	R	0.072	A	<0.01	R	0.007	R
PSF-5	0.026	R	0.284	A	<0.01	R	0.203	A
PSF-6	0.173	A	0.490	A	0.017	R	≥0.25	A
PSF-7	0.354	A	0.116	A	0.212	A	≥0.25	A
PSF-8	0.001	R	0.074	A	<0.01	R	0.040	R
PSF-9	0.000	R	0.234	A	<0.01	R	0.056	A
PSF-10	0.004	R	0.583	A	<0.01	R	≥0.25	A
PSF-11	0.000	R	0.234	A	<0.01	R	0.056	A
PSF-12	0.033	R	0.731	A	<0.01	R	≥0.25	A
PSF-13-15	0.000	R	0.133	A	<0.01	R	0.015	R

Table 4. Estimated experimental SBS conditions and responses from particular values of desirability.

Desirability	Work distance (cm)	Feed rate (mL/min)	Air pressure (bar)	Theoretical RoF (%)	Theoretical DoF (nm)
1.00	**20.0**	**0.375**	**2.2**	**97**	**142**
0.89	20.0	0.375	1.5	88	157
0.87	25.0	0.219	2.1	88	160
0.84	24.7	0.212	2.1	84	162
0.73	22.5	0.250	2.0	79	171
0.63	24.7	0.341	1.6	82	186
0.60	20.2	0.375	1.0	73	183
0.52	25.0	0.375	3.0	90	201
0.46	**25.0**	**0.125**	**3.0**	**65**	**196**
0.29	20.1	0.141	1.2	64	211
0.15	**22.5**	**0.125**	**3**	**41**	**211**

Table 5. Contact angles obtained on three of the samples prepared by SBS.

Sample	**θ_{Water} (º)**		**$\theta_{Glycerol}$ (º)**	
PSF-6	159.5±3.5	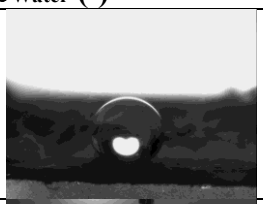	158.6±8.0	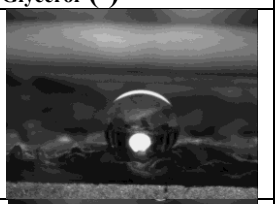
PSF-2	151.9±4.5		148.1±4.8	
PSF-11	147.6±5.0	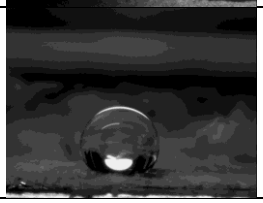	135.2±5.0	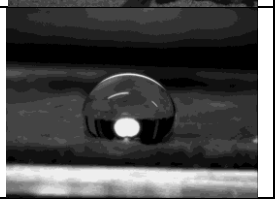

Table 6. Arithmetical mean roughness, R_a, roughness factor, r, and fraction of solid surface in direct contact with the liquid, φ_s.

Sample	**R_a (μm)**	**r**	**φ_S**
PSF-6	8.4 ± 3	1.18 ± 0.10	0.96
PSF-2	5.8 ± 2	1.21 ± 0.15	0.85
PSF-11	6.4 ± 3	1.13 ± 0.10	0.86